Lightning Grounding Grid Model Considering Both the Frequency-Dependent Behavior and Ionization Phenomenon

Hongcai Chen , *Student Member, IEEE* and Yaping Du

***Abstract*—A grounding grid is essential to the lightning protection of power systems. This paper presents a modified partial element equivalent circuit method for predicting the transient behavior of the grounding grid. The frequency-dependent parameters of the grounding grid are obtained first by using the image method. Both modified nodal formulation and vector fitting techniques are applied to derive an extended equivalent network for time-domain simulation. In this method, the soil ionization effect is considered using a nonlinear resistance. The proposed method is verified with experimental results available in the literature. Finally, lightning transients in the grounding grid of a radio base station is presented. The ionization and propagation effects on grounding grid performance are discussed.**

***Index Terms*—Equivalent circuit, grounding grid, lightning transient, partial element equivalent circuit (PEEC), soil ionization.**

I. Introduction

GROUNDING grid performance is one of major concern of lightning protection for power systems. An effective grounding grid can direct the lightning current to the earth with a low potential rise. The analysis of grounding grids during a lightning strike has been widely investigated using both analytical expressions and numerical techniques. The models developed for grounding transient analysis can be classified in three categories: circuit model, transmission line model, and electromagnetic field model.

The circuit model [1]–[5] represents a grounding electrode as a lumped *RLC* equivalent circuit. Mutual inductance, capacitance, and resistance are brought to model coupling effects among different grounding conductors. The nonlinear soil ionization effect can be incorporated into the model. However, the main drawback of the circuit model is that it is difficult to deal with frequency-variant parameters. The transmission line model [6]–[8] was initially deduced by Sunde and has been popular ever since. This method uses Bergeron's travelling wave technique to derive the frequency-dependent impedance of a grounding electrode. The model can be also analyzed in time domain, thus is capable of including the soil ionization effect. The electromagnetic field model [9]–[13], which is strictly based on the electromagnetic theory, is considered as the most rigorous method to model the transient behavior in a grounding electrode. This method is a frequency-domain approach which limits its application only for linear systems. Therefore, this method cannot include nonlinear soil ionization phenomena efficiently. Meanwhile, the field approach needs huge computer memory and computation time in simulation.

Soil ionization phenomena are observed locally around an electrode in the situations of a large impulse injected to the ground. The behavior of the electrode is completely different from that at the low-level excitation. Recently ionization models have been developed for transient analysis in the ground [14]–[18]. Empirical expressions for modeling the ionization effect were well proposed, including the nonlinear resistance model. Note that the model itself is not able to take into account the frequency characteristics of a grounding electrode.

Frequency-dependent soil parameter [19]–[22] is another important influence factor on the ground grid. Previously, this effect has been neglected in evaluating the performance of grounding grids due to the lack of formulations to describe it. While, Visacro and Alipio [20] proposed the formulation for expressing soil parameter frequency dependence based on laboratory and field measurements. He also revealed that frequency dependence of the soil parameters results in a decrease of the potential of the grounding electrode, with respect to the case where the parameters are assumed to be constant.

Though many models have been developed for a grounding electrode, predicting the transient performance of a grounding system is still a challenging issue. In this paper, a modified partial element equivalent circuit (PEEC) method is proposed to model and analyze transients in a grounding grid. The vector fitting method [23], [24] is adopted and the ionization resistance is included to deal with the frequency- and current-dependent characteristics of the grounding grid. The modified PEEC formulation including techniques dealing with frequency- and current-dependent parameters is described in Section II. Section III presents the validation of the proposed model by comparing with experimental results available in the literature. Finally, the grounding grid for a radio base station (RBS) is investigated, and the effect of the ionization phenomenon and soil resistivity is discussed.

This work was supported by the grants from the Research Grants Council of the HKSAR under Project 152038/15E and Project 152100/17E. *(Corresponding author: Hongcai Chen.)*

The authors are with the Department of Building Services Engineering, The Hong Kong Polytechnic University, Hong Kong (e-mail: hc.chen@live.com; ya-ping.du@polyu.edu.hk).

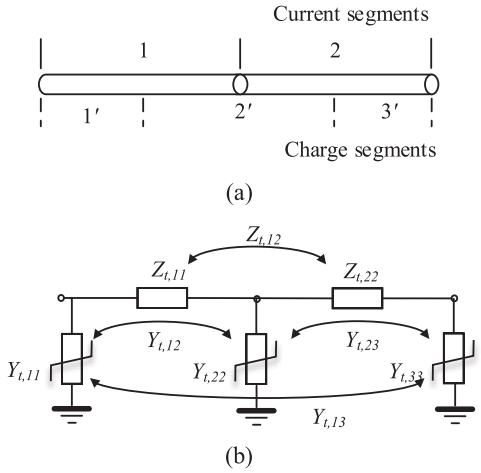

Fig. 1. Segments and equivalent circuits of a grounding electrode. (a) Wire segments. (b) Equivalent circuit of the segments.

II. Basic Ground Impedance Formulation

Transients in a grounding grid are more complex than those in the conductors above the ground. Two issues may be addressed in the transient analysis of a grounding grid, that is, wave propagation and soil ionization. The propagation effects are frequency dependent and could be effectively analyzed using the electromagnetic theory. Soil ionization occurs when the current impulse has a high magnitude, which results in a low ground resistance. Under this situation, the electric field at the electrode surface is greater than the ionization threshold. To include both propagation phenomena and soil ionization in the analysis, frequency- and current-dependent characteristics of the grounding grid should be implemented simultaneously.

A. PEEC Model of Grounding Electrodes

The PEEC method [25]–[27] has been developed for modeling electromagnetic coupling among thin conductors. It represents the electric field integral equation using an equivalent circuit which can be integrated into a circuit solver directly.

In the PEEC method, all the conductors need to be divided into small segments for taking into account the nonuniform distributions of the current and the charge. In the T-type circuit model, both current and charge segments are offset with half-length of a segment, as seen in Fig. 1(a). The segment length is commonly chosen as one-tenth of the wavelength in the soil at the primary frequency of concern. In this method both volume currents and surface charges or voltages on the segments [28] are the unknown parameters to be determined.

Fig. 1(b) shows an equivalent circuit for the conductor given in Fig. 1(a). Current segments of the conductor are represented with longitudinal impedances, i.e., self-impedance $Z_{t,ii}$ and mutual impedance $Z_{t,ij}$ (i and $j = 1, 2, \ldots$). The self-impedance is made up of internal impedance and external impedance. Because segment current is not evenly distributed over the cross section due to the skin effect, frequency-variant formulas are adopted to determine the internal impedance of a segment. For a solid circular segment with radius a, internal impedance $Z_{t,ii,s}$ is expressed as [6], [29], [30]

$$Z_{t,ii,s} = \frac{j\omega}{2\pi R_a}\frac{I_0(R_a)}{I_1(R_a)} \tag{1}$$

where $I_k(\cdot)$ is the modified Bessel function of order k, and $R_a = \sqrt{j\omega\sigma\mu}\cdot a$. Both σ and μ are the conductivity and permeability of the conductor. In case of a segment with noncircular cross section, a two-dimensional eddy-current analysis procedure [31] needs to be applied to determine its internal impedance.

External impedance $Z_{t,ii,e}$ of a segment is determined using surface current on the segment. As the soil is assumed to be a nonmagnetic material which is the same as the air, external impedance of a segment in the soil has the same expression as that in the air. A general procedure for the conductor with arbitrary cross section is presented in the appendix of [31].

It is noted that conductor spacing in a grounding grid is usually much greater than its cross-sectional dimensions. Mutual inductance of two segments is simply determined using the filament model, and is expressed as [32]

$$Z_{t,ij} = j\omega\frac{\mu_0}{4\pi}\int_{\Gamma_i}\int_{\Gamma_j}\frac{\vec{dl_i}\cdot\vec{dl_j}}{R_{ij}} \tag{2}$$

where μ_0 is the permeability of the soil. Both Γ_i and Γ_j are the lines of segment i and j, and R_{ij} is the distance between two segments. For two parallel segments with spacing d_0 and length l_0, an explicit formula yields, as follows:

$$Z_{t,ij} = j\omega\frac{\mu_0 l_0}{4\pi}\left[\ln\left(\frac{l_0}{d_0}+\sqrt{1+\frac{l_0^2}{d_0^2}}\right)-\sqrt{1+\frac{d_0^2}{l_0^2}}+\frac{d_0}{l_0}\right]. \tag{3}$$

Impedance matrix $\mathbf{Z}_{\mathrm{T}}$ can be then constructed by assembling self and mutual impedances given in (1)–(3).

Charge or potential segments are represented with transverse admittance, as shown in Fig. 1(b). It represents the leaking current from the grounding grid in the soil, and is a function of the soil properties and the electrode geometry. As the earth is assumed to be a semi-infinite medium, the image method [1] is adopted for the calculation. The air is replaced with the image of each segment. Taking the fact that the conductivity and the relative permeability of the air is 0 and 1, coefficient of potential $p_{t,ij}$ on segment i contributed by charge on segment j is given as

$$p_{t,ij} = \frac{j\omega}{4\pi\left(\sigma_g + j\omega\varepsilon_g\right)l_i l_j} \cdot\left[\int_{\Gamma_i}\int_{\Gamma_j}\frac{1}{R_{ij}}dl_i dl_j + k_g\cdot\int_{\Gamma_{i'}}\int_{\Gamma_j}\frac{1}{R_{i'j}}dl_{i'}dl_j\right] \tag{4}$$

where reflection coefficient k_g is expressed as

$$k_g = \frac{\sigma_g + j\omega\ \varepsilon_g - \varepsilon_0)}{\sigma_g + j\omega\ \varepsilon_g + \varepsilon_0)}.$$

In (4) both σ_g and ε_g are, respectively, the conductivity and permeability of the soil. $\Gamma_{i'}$ is the line of segment image i,' and $R_{i'j}$ is the distance between segment image i' in air and segment

j under the ground. Admittance matrix $\mathbf{Y}_\mathrm{T}$ is then obtained by inverting matrix $\mathbf{P} = [p_{t,ij}]$, i.e., $\mathbf{Y}_\mathrm{T} = j\omega\mathbf{P}^{-1}$.

B. Soil Ionization Effect

When a substantial lightning current is discharged via a grounding electrode, electric field around the electrode may exceed the breakdown strength of the soil. This results in a low-resistance zone in the vicinity of the electrode. The ionization effect, which depends on electrical and geometrical parameters, can be simulated approximately using a nonlinear resistance resulting from a virtual electrode with current-varying radius [33]. The radius of the virtual electrode increases until the electric field around the electrode does not exceed the breakdown strength of the soil. An empirical formula for the nonlinear resistance as a function of the injected current pulse has been recommended by CIGRE [17], and is expressed as

$$R_g(I) = \frac{R_0}{\sqrt{1 + I(t)/I_g}} \tag{5}$$

where $I_g = E_0/2\pi\sigma_g R_0^2$, and $I(t)$ is the current injected into the electrode. E_0 is the critical electric field intensity of the soil, and R_0 is the ground resistance with low current at low frequency.

C. Extended Equivalent Circuit Model

With impedance and admittance matrices $\mathbf{Z}_\mathrm{T}$ and $\mathbf{Y}_\mathrm{T}$ of the grounding grid, a matrix equation can be established using the modified nodal analysis formulation, as follows:

$$\begin{bmatrix} -\mathbf{A} & \mathbf{Z_T} \\ \mathbf{Y_T} & -\mathbf{A^T} \end{bmatrix} \begin{bmatrix} \mathbf{I} \\ \Phi \end{bmatrix} = \begin{bmatrix} \mathbf{V_s} \\ \mathbf{I_s} \end{bmatrix} \tag{6}$$

where $\mathbf{A}$ is the incidence matrix of the original network. Formulation (6) is set up in frequency domain as both self-impedance and admittance vary with frequency. In order to perform a time-domain simulation, an extended network built with frequency-invariant circuit components is constructed using a rational approximation technique.

Note that the network built with (6) consists of two independent parts: impedance subnetwork for matrix $\mathbf{Z}_\mathrm{T}$ and admittance subnetwork from matrix $\mathbf{Y}_\mathrm{T}$. These two subnetworks share the common nodes, and can be converted into the extended subnetworks individually by the vector fitting technique. The final extended network can be then assembled by combining these extended subnetworks together.

Fig. 2 shows these two subnetworks for two coupled branches. Impedance subnetwork retains the original topology of the branches. It contains original self- and mutual- impedance models of the branches. The admittance network retains the nodes in the original network. The original coefficients of potential among the nodes in admittance matrix $\mathbf{Y}_\mathrm{T}$ can be realized with an electrical circuit without mutual coupling, as shown in Fig. 2. Assume that Y_{ij} is the admittance of the equivalent branch between nodes i and j, and Y_{ii} is the admittance of the equivalent

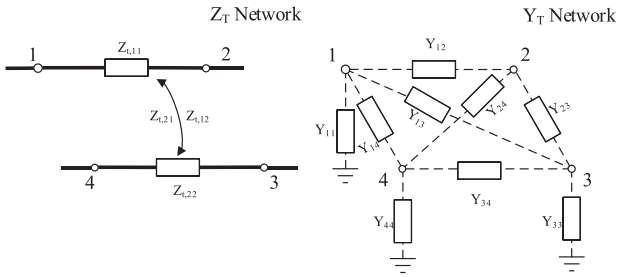

Fig. 2. Equivalent network of two coupled branches in the soil.

branch between node i and the reference. They are expressed as

$$\begin{aligned} Y_{ij} &= -Y_{t,ij} \\ Y_{ii} &= Y_{t,ii} - \sum\nolimits_{j=1}^{n} Y_{t,ij}. \end{aligned} \tag{7}$$

The mutual coupling effect in the original equation now is replaced with admittance of equivalent branches connected to these nodes defined in the original network.

In the network shown in Fig. 2, both self-impedance Z_{ii} and admittance Y_{ij} are frequency dependent. Z_{ii} in s domain can be approximated by rational functions in rational polynomial, pole-zero or pole-residue form, as

$$Z_{ii}(s) = R_{ii,0} + sL_{ii,0} + \sum_{m=1}^{M} \frac{s}{s - a_{ii,m}} r_{ii,m} \tag{8}$$

where $R_{ii,0}$, $L_{ii,0}$, $a_{ij,m}$, and $r_{ij,m}$ in the following equation are the constants obtained using a data fitting approach, such as the vector fitting or least-squares fitting method. Similarly, Y_{ij} can be approximated by the following rational functions as well

$$Y_{ij}(s) = G_{ij,0} + sC_{ij,0} + \sum_{m=1}^{M} \frac{1}{s - b_{ij,m}} r_{ij,m}. \tag{9}$$

Constants $G_{ij,0}$, $C_{ij,0}$, $b_{ij,m}$, and $r_{ij,m}$ in (8) are also obtained using a data fitting approach. These rational functions can be realized with the Mth order RL and RC circuits, respectively [34]–[36]. Fig. 3 shows the realized circuits for the rational functions given in (7) and (8). In Fig. 3 circuit parameters of all the components are frequency invariant.

According to (9), $G_{ii,0}$ could be considered as the conductance of grounding segment i under a dc current. Thus, element for $G_{ii,0}$ is represented as a resistor with the resistance that equals to dc ground resistance of the segment. In order to incorporate the ionization effect in the circuit analysis, this resistance is approximated by nonlinear resistance $R_{g,i}(I)$ given in (5). Now the original grounding grid is completely replaced with an extended circuit network built up using frequency-invariant circuit components together with a number of nonlinear resistances. Subsequently, the time-domain simulation can be performed by using a conventional circuit analysis approach.

III. Verification of the Model

The model described in this paper has been verified by the comparison with several experimental tests extracted from the

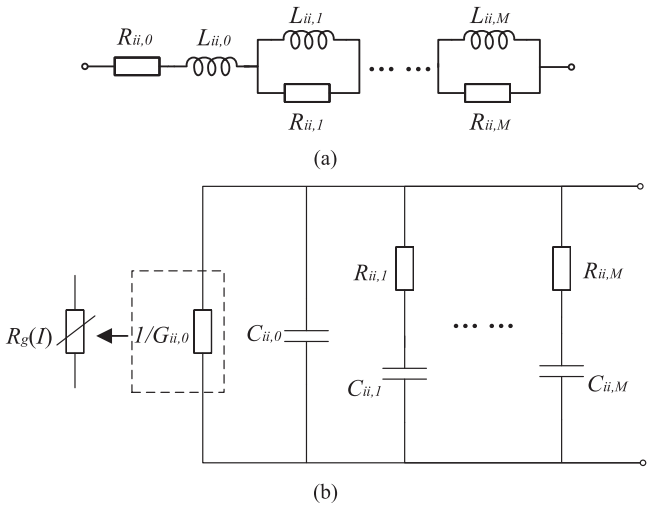

Fig. 3. Rational equivalent circuit of (a) Z_{ii} where $R_{ii,m} = -r_{ii,m}/a_{ii,m}$, and $L_{ii,m} = 1/r_{ii,m}$, and (b) Y_{ii} where $R_{ii,0} = 1/G_{ii,0}$, $R_{ii,m} = -r_{ii.m}/b_{ii,m}$, and $C_{ii,m} = 1/r_{ii,m}$.

TABLE I
INFORMATION OF ELECTRODES AND THE SOIL

	Material	Radius (mm)	Length (m)	Depth (m)	ρ_g (Ω·m)	ε_g
Vertical	steel	10	6	–	50	8
Horizontal	copper	6	15	0.6	80	15

published literature. First, the transient behavior of simple electrodes under low impulse currents is compared for verifying the modeling of frequency-dependent effects. Then, the behavior under high impulse currents is demonstrated to show the performance of the model when soil ionization occurs. Finally, the transient results on a 2 m × 2 m grounding grid are presented for comparison. The experimental data or curves for comparison were manually sampled from figures or graphs available in the published literature. The sampled currents used as the source in the circuit solver were processed with a 10 MHz low-pass filter first. In all the simulations, the breakdown strength of soil was assumed as $E_0 = 350\,\mathrm{kV/m}$.

A. Low-Current Measurements by Électricité de France [7]

A 6-m-long vertical rod and a 15-m-long horizontal wire were separately tested under small impulse excitation. Steep impulse currents with the front time of less than 0.5 μs were injected at one end of the electrodes. The parameters of the electrodes and the soil are listed in Table I. The transient voltages at the injection point in both cases were measured, as well as at the points of 3.5 and 7 m from that point along the horizontal electrode.

The results by measurement and simulation are presented in Figs. 4 and 5. It is found that they agree with each other generally. Some differences in the voltage peak and voltage waveform are observed, which might be caused by two things. First, the propagation effects of the impulse are underestimated which are dominant under the fast impulse fronts. In these fast transients, the frequency can reach up to 10 MHz that a slight change of

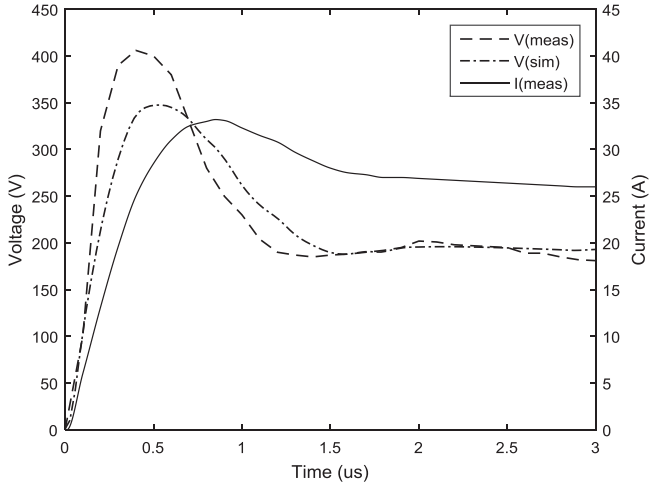

Fig. 4. Transient voltages on a 6 m vertical rod under a small impulse current. (meas. – measurement, sim. – simulated result).

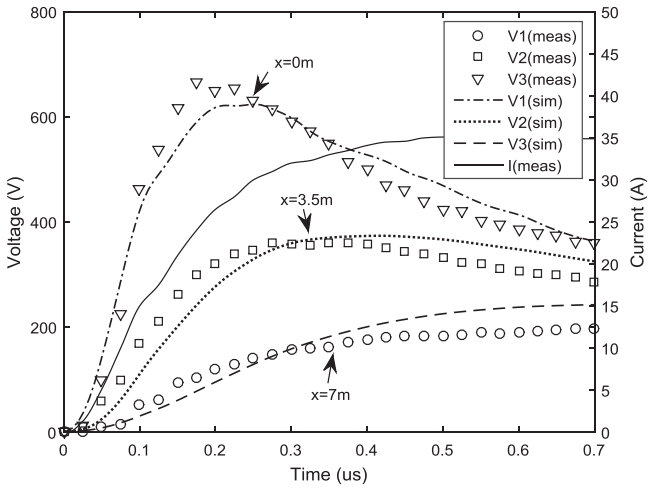

Fig. 5. Transient voltages on a 15 m horizontal wire under a small impulse current. (meas. – measurement, sim. – simulated result).

TABLE II
INFORMATION OF ELECTRODES AND THE SOIL

	Material	Radius (mm)	Length (m)	Depth (m)	ρ_g (Ω·m)	ε_g
Vertical	steel	25	1	–	42	10
Horizontal	steel	4	5	0.6	42	10

inductance would lead to large errors in voltage calculation. Second, the source current was obtained by point-by-point sampling which could result in errors in the waveform of an impulse.

B. High-Current Measurements by Geri [37]

In this part, the impulses with peak current more than 25 kA were injected separately into a 1-m-long vertical rod and a 5-m-long horizontal wire for comparison. Soil ionization phenomena were expected under such high-current levels. The parameters of two grounding electrodes are listed in Table II. Figs. 6 and 7 show both measured currents and voltages at the injection point

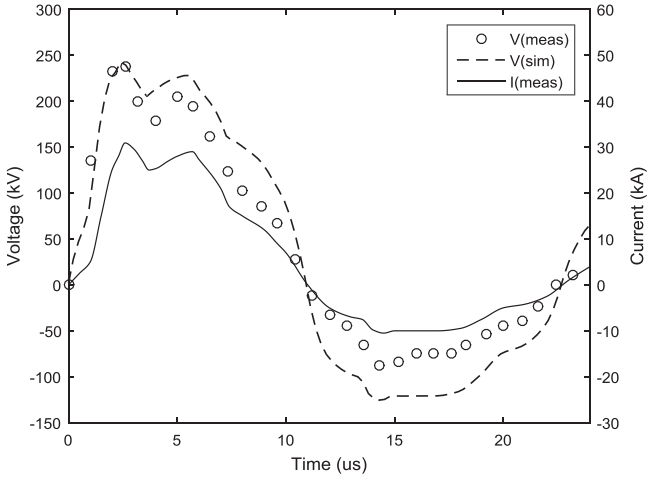

Fig. 6. Transient voltages on a 1 m vertical rod under a large impulse current. (meas. – measurement, sim. – simulated result).

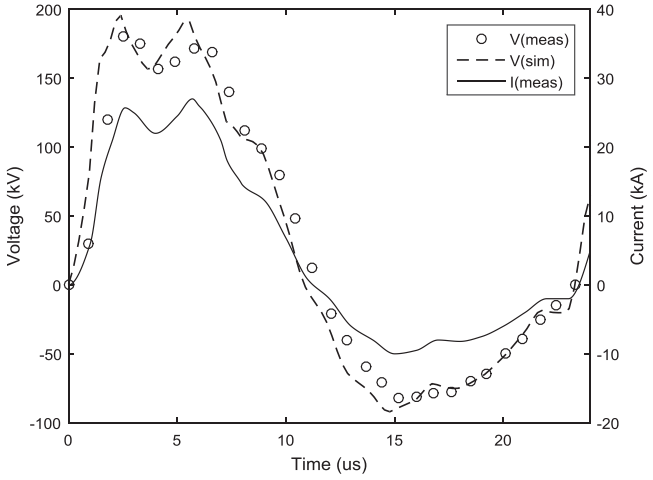

Fig. 7. Transient voltages on a 5 m horizontal wire under a large impulse current. (meas. – measurement, sim. – simulated result).

of electrodes under such large impulse currents. It is found that the simulation results match well with the measurement results. Again, point-by-point sampling of the source current from the literature may introduce errors in the slope of the waveforms.

C. Measurement on a Grounding Grid by Stojkovic et al. [38]

A 2 m × 2 m horizontal grounding grid with the dimensions of 10 m × 10 m was selected for comparison. The grid was made of round copper wires with the cross section of 50 mm^2. It was buried 0.5 m underground. The soil resistivity was estimated to be 29.1 Ω·m [38]. The impulse with a peak current of 10 A was injected at one corner of the grid. Both the transient voltage and the transient current at the injection point were measured. Fig. 8 shows the comparison of the transient voltages obtained from the calculation and the simulation. It is found that the calculated and measured voltages match well in waveform, and the difference of their peak values is less than 3%. Therefore, the proposed model for grounding grids is generally acceptable for the simulation of transients during a lightning stroke.

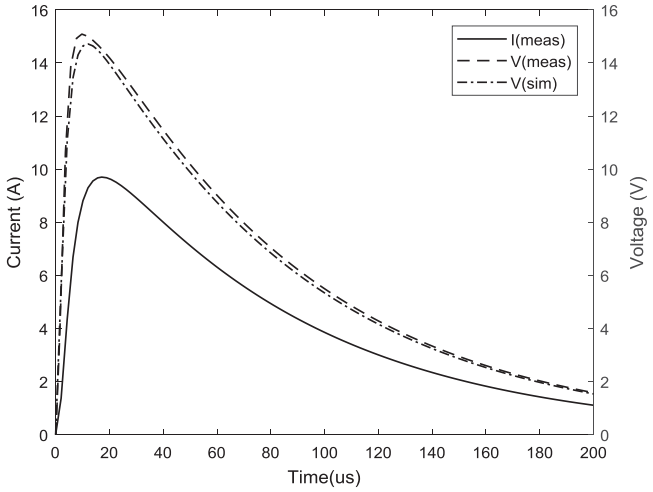

Fig. 8. Transient voltages on a 2 m × 2 m grounding grid. (meas. – measurement, sim. – simulated result).

TABLE III
PARAMETERS OF THE TWO HEIDLER'S FUNCTIONS

	i_{max} (kA)	Waveform	η	T (μs)	τ (μs)
First Stroke	200	10/350	0.93	19	485
Subsequent Stroke	50	0.25/100	0.993	0.454	143

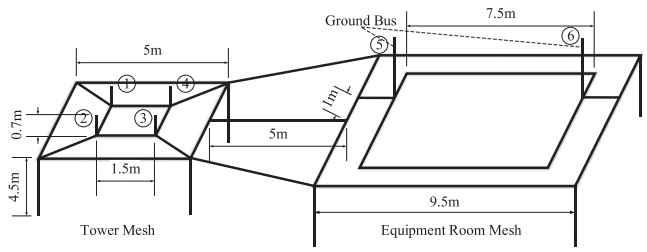

Fig. 9. Configuration of the grounding grid for radio base system.

IV. ANALYSIS OF THE GROUNDING GRID FOR AN RBS

In this section, analysis of the grounding grid for RBS is presented under direct lightning strokes. In the analysis, the lightning current impulses specified in IEC Standard 62305 [39] are adopted. These impulses can be expressed using Heidler's equation [40] as

$$i(t) = \frac{i_{max}}{\eta} \frac{(t/T)^n}{1+(t/T)^n} \exp(-t/\tau) \tag{10}$$

where η is the correction coefficient of the current peak i_{max}, T is the front-time coefficient, τ is the stoke duration time, and n is the current steepness factor. Two different current waveforms are tested, that is, the first and subsequent lightning stroke current waves. The first stroke current has larger intensity, while the subsequent stroke current has a larger rate in its front. The constants in (10) for these two lightning stroke currents are shown in Table III.

Fig. 9 shows the configuration of a practical grounding grid for an RBS. The grounding grid consists of a tower mesh of 5 m × 5 m buried at 0.7 m depth and an equipment-room mesh

TABLE IV
MATERIAL INFORMATION OF TOWER AND THE ROD

Material	u_r	Rdc (Ω/m)	Radius (mm)
Horizontal Grid	42	0.24	19
Vertical Rod	42	0.15	23.5

of 9.5 m × 9.5 m buried also at the same depth. Two meshes are interconnected via three horizontal conductors. Meanwhile, eight vertical rods of 4.5 m in length are provided at the corners of tower and room meshes. The ground buses are connected to the equipment-room mesh at two ends of the room. The soil resistivity is taken to be 100 Ω·m, and an additional value of 1000 Ω·m is selected for comparison. The relative permittivity of soil is assumed to be 10. The critical electric field is assumed to be 350 kV/m. The material of the conductors used in the grid is listed in Table IV.

The impulse currents are injected into the grounding grid from rods ①, ②, ③, and ④ simultaneously, which are connected to four feet of the telecommunication tower. ⑤ is the ground bus outside the equipment room, which provide the grounding for power/signal cables. The potential difference between four foot rods and the ground bus ⑤ is investigated. Ground potential rise at these points, as the result of the impulse current in the grounding grid, was evaluated with the proposed procedure. The calculations with and without ionization are presented to investigate the influence of the ionization phenomenon. Meanwhile, the propagation effect of the lightning pulse in the grounding grid is also discussed by comparing waveforms under first and subsequent strokes.

Figs. 10 and 11 show potentials at Point ① and Point ⑤ on the ground grid with and without considering the soil ionization, as well as the potential difference between these two points. Both 100 and 1000 Ω·m soil resistivities are considered in the simulation. The injected current is either the 200 kA first lightning stroke current or the 50 kA subsequent lightning stroke current.

By comparing Fig. 10(a) with (b), it is found that the potential difference between the models with and without ionization becomes larger when the soil resistivity is 1000 Ω·m. This indicates that the ionization affects more significantly when the soil resistivity is higher under the first stroke. The behavior under the subsequent stroke also gives the same result as shown in Fig. 11(a) and (b).

Fig. 11 shows a large peak potential in the beginning of the potential waveform, where corresponds to wavefront. However, this peak potential lasts only during the wavefront of the current impulse and then deceases quickly to a stationary period. It reveals that the subsequent stroke is greatly affected by the propagation behavior of a lightning impulse. By comparing the waveform shapes of ionization and nonionization results in Fig. 11(a) and (b), we can find that propagation effect is barely influenced by the ionization effect and the soil resistivity.

As shown in Fig. 10(c) and (d), the peak potential difference between the foot rod and the ground bus reaches, respectively, 113 and 81 kV for ionization and nonionization cases when

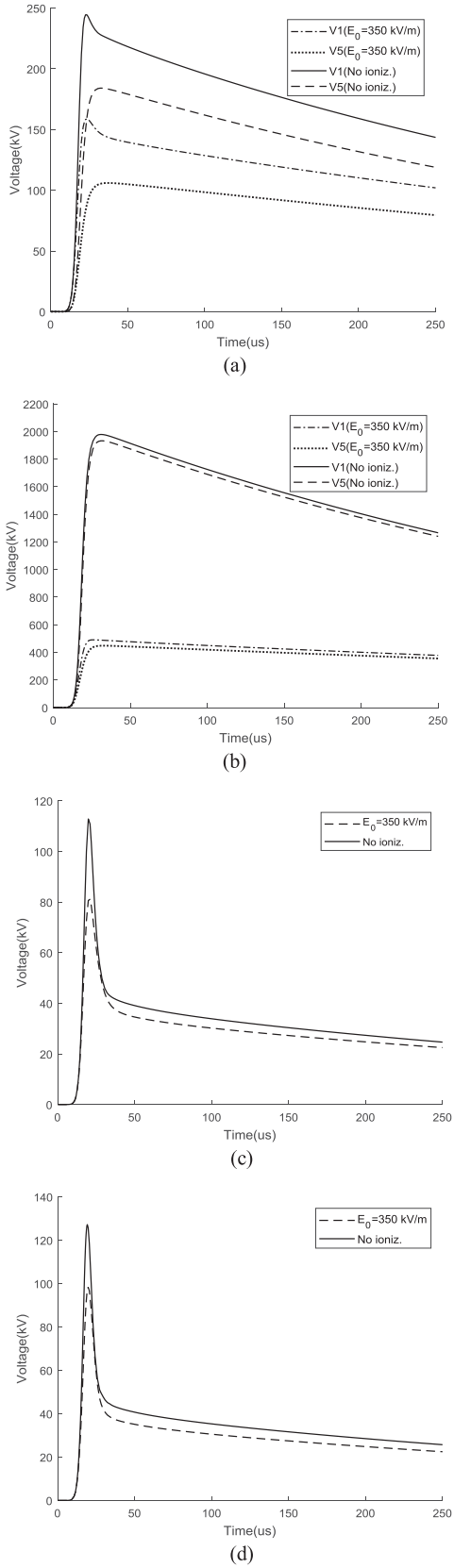

Fig. 10. Comparison of potentials with and without ionization effect under a 10/350 μs impulse with a peak current of 200 kA. (a) Potentials at ① and ⑤, $R_g = 100\,\Omega\cdot$m. (b) Potentials at ① and ⑤, $R_g = 1000\,\Omega\cdot$m. (c) Potential difference between ① and ⑤, $R_g = 100\,\Omega\cdot$m. (d) Potential difference between ① and ⑤, $R_g = 1000\,\Omega\cdot$m. (No Ioniz. – without ionization effect).

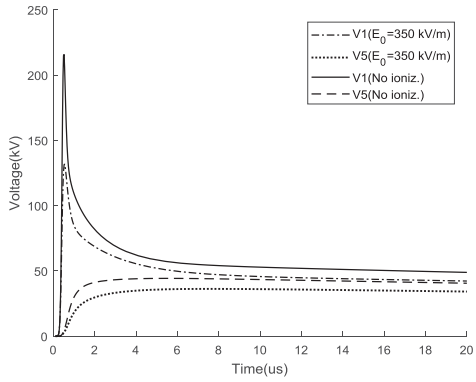

(a)

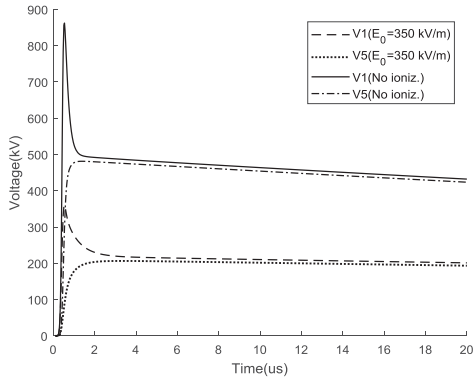

(b)

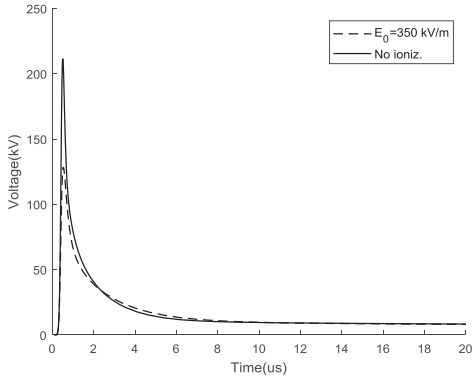

(c)

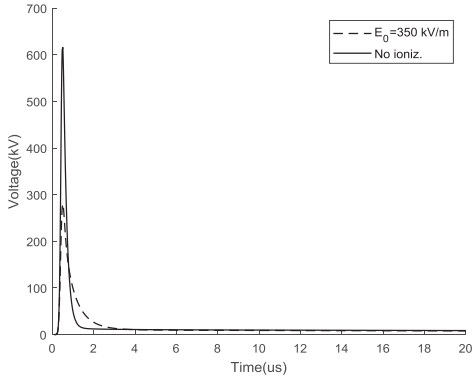

(d)

Fig. 11. Comparison of potentials with and without ionization effect under 0.25/100 μs impulse with a peak current of 50 kA. (a) Potentials at ① and ⑤, $R_g = 100\,\Omega{\cdot}$m. (b) Potentials at ① and ⑤, $R_g = 1000\,\Omega{\cdot}$m. (c) Potential difference between ① and ⑤, $R_g = 100\,\Omega{\cdot}$m. (b) Potential difference between ① and ⑤, $R_g = 1000\,\Omega{\cdot}$m. (No Ioniz. – without ionization effect).

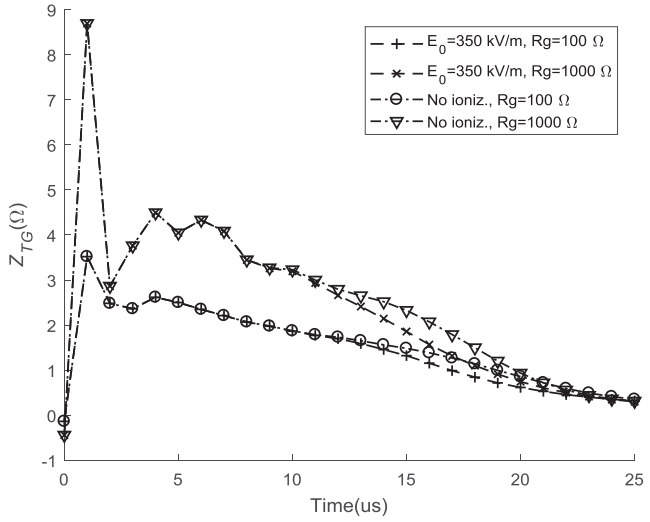

(a)

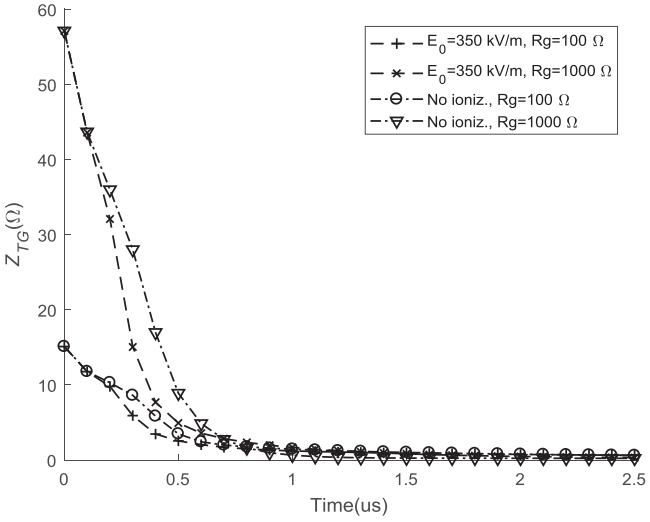

(b)

Fig. 12. Transient ground impedance between point ① and ⑤ with and without ionization effect at the rise front of lighting impulses. (a) Under 10/350 μs impulse. (b) Under 0.25/100 μs impulse. (No Ioniz. – without ionization effect).

soil resistivity is 100 Ω·m. However, the difference becomes, respectively, 127 and 98 kV when soil resistivity increases to 1000 Ω·m. Therefore, the potential difference varies little when soil resistivity changes under the first stroke.

However, the peak potential difference between points ① and ⑤ varies significantly under the subsequent stroke with the fast rise front. This is because the contribution of both propagation effect and high soil resistivity. Due to the limited speed of lightning propagation in the grounding grid, only a small part of the grounding grid is effective in discharging the current to the earth in the wavefront. Thus, potential difference comes to its maximum before the soil ionization is fully developed. High soil resistivity will reinforce this effect as the potential at early arrived point has higher values when soil resistivity grows.

Fig. 12 shows the time variant of the transient grounding impedance between the foot rod and ground bus. The transient grounding impedance (Z_{TG}) is a time function defined as a

quotient between $v(t)$ and $i(t)$ as $Z_{\mathrm{TG}}(t) = v(t)/i(t)$. The Z_{TG} at the waveform front is mainly caused by the propagation effect. As a first approximation [17], the first stroke current waveform's frequency content is below 100 kHz, and subsequent stroke's is below 1 MHz. Thus, subsequent stroke suffers more from the propagation effect, which behaves as a higher transient ground impedance as displayed in Fig. 12(b). By comparing the results with/without ionization effect we can find that transient ground impedance with/without ionization almost coincident with each other. It proved that soil ionization does not have a large effect in reducing the propagation potential peak. The transient ground impedance between feet rod and room bus under these two stroke waveforms decrease to about 0.2 Ω quickly after the front of the waveform. Under the first stroke, the ionization effect is more significant than the propagation effect because of its low-frequency spectrum.

V. Conclusion

In this paper, we proposed a modified PEEC method for transient simulation of the grounding grid. The techniques of modified nodal network transformation and rational approximation were employed to generate a time-domain equivalent network. Ionization effect was also taken into consideration by using a nonlinear resistance. The proposed approach was verified experimentally, and was applied to evaluate lightning potential distribution in a practical grounding grid for an RBS system.

The behavior of the grounding grid is affected by both ionization and propagation effects. The analysis shows that the ionization effect decides the performance of the grounding grid under first stroke. While, the propagation effect is dominant for the wavefront of the subsequent stroke. The potential difference between the tower footing and the equipment room barely varies with the soil resistivity under the first stroke. However, under the subsequent stroke, the potential difference is greatly affected by the soil resistivity because of the propagation effect.

References

[1] A. F. Otero, J. Cidras, and J. L. del Alamo, "Frequency-dependent grounding system calculation by means of a conventional nodal analysis technique," *IEEE Trans. Power Del.*, vol. 14, no. 3, pp. 873–878, Jul. 1999.

[2] R. Zeng, X. H. Gong, J. L. He, B. Zhang, and Y. Q. Gao, "Lightning impulse performances of grounding grids for substations considering soil ionization," *IEEE Trans. Power Del.*, vol. 23, no. 2, pp. 667–675, Apr. 2008.

[3] F. M. Gatta, A. Geri, S. Lauria, and M. Maccioni, "Simplified HV tower grounding system model for backflashover simulation," *Elect. Power Syst. Res.*, vol. 85, pp. 16–23, 2012.

[4] G. Celli, E. Ghiani, and F. Pilo, "Behaviour of grounding systems: A quasi-static EMTP model and its validation," *Elect. Power Syst. Res.*, vol. 85, pp. 24–29, 2012.

[5] Z. Feng, X. Wen, X. Tong, H. Lu, L. Lan, and P. Xing, "Impulse characteristics of tower grounding devices considering soil ionization by the time-domain difference method," *IEEE Trans. Power Del.*, vol. 30, no. 4, pp. 1906–1913, Aug. 2015.

[6] E. D. Sunde, *Earth Conduction Effects in Transmission Systems*. New York, NY, USA: Dover, 1968.

[7] F. Mentre and L. Grcev, "EMTP-based model for grounding system analysis," *IEEE Trans. Power Del.*, vol. 9, no. 4, pp. 1838–1849, Oct. 1994.

[8] Y. Q. Liu, M. Zitnik, and R. Thottappillil, "An improved transmission-line model of grounding system," *IEEE Trans. Electromagn. Compat.*, vol. 43, no. 3, pp. 348–355, Aug. 2001.

[9] L. Grcev and F. Dawalibi, "An electromagnetic model for transients in grounding systems," *IEEE Trans. Power Del.*, vol. 5, no. 4, pp. 1773–1779, Oct. 1990.

[10] F. Dawalibi, A. Selby, and R. G. Olsen, "Electromagnetic-fields of energized conductors," *IEEE Trans. Power Del.*, vol. 8, no. 3, pp. 1275–1284, Jul. 1993.

[11] L. D. Grcev, "Computer analysis of transient voltages in large grounding systems," *IEEE Trans. Power Del.*, vol. 11, no. 2, pp. 815–823, Apr. 1996.

[12] L. Qi, X. Cui, Z. Zhao, and H. Li, "Grounding performance analysis of the substation grounding grids by finite element method in frequency domain," *IEEE Trans. Magn.*, vol. 43, no. 4, pp. 1181–1184, Apr. 2007.

[13] H. Karami, K. Sheshyekani, and F. Rachidi, "Mixed-potential integral equation for full-wave modeling of grounding systems buried in a lossy multilayer stratified ground," *IEEE Trans. Electromagn. Compat.*, vol. 59, no. 5, pp. 1505–1513, Oct. 2017.

[14] A. C. Liew and M. Darveniza, "Dynamic model of impulse characteristics of concentrated earths," *Proc. Inst. Elect. Eng.-London*, vol. 121, no. 2, pp. 123–135, 1974.

[15] A. Geri, G. Veca, E. Garbagnati, and G. Sartorio, "Non-linear behaviour of ground electrodes under lightning surge currents: Computer modelling and comparison with experimental results," *IEEE Trans. Magn.*, vol. 28, no. 2, pp. 1442–1445, Mar. 1992.

[16] S. Sekioka, M. I. Lorentzou, M. P. Philippakou, and J. M. Prousalidis, "Current-dependent grounding resistance model based on energy balance of soil ionization," *IEEE Trans. Power Del.*, vol. 21, no. 1, pp. 194–201, Jan. 2006.

[17] L. Grcev, "Modeling of grounding electrodes under lightning currents," *IEEE Trans. Electromagn. Compat.*, vol. 51, no. 3, pp. 559–571, Aug. 2009.

[18] J. L. Li, T. Yuan, Q. Yang, W. X. Sima, C. X. Sun, and M. Zahn, "Numerical and experimental investigation of grounding electrode impulse-current dispersal regularity considering the transient ionization phenomenon," *IEEE Trans. Power Del.*, vol. 26, no. 4, pp. 2647–2658, Oct. 2011.

[19] S. Visacro, R. Alipio, M. H. Murta Vale, and C. Pereira, "The response of grounding electrodes to lightning currents: The effect of frequency-dependent soil resistivity and permittivity," *IEEE Trans. Electromagn. Compat.*, vol. 53, no. 2, pp. 401–406, May 2011.

[20] S. Visacro and R. Alipio, "Frequency dependence of soil parameters: Experimental results, predicting formula and influence on the lightning response of grounding electrodes," *IEEE Trans. Power Del.*, vol. 27, no. 2, pp. 927–935, Apr. 2012.

[21] R. Alipio and S. Visacro, "Frequency dependence of soil parameters: Effect on the lightning response of grounding electrodes," *IEEE Trans. Electromagn. Compat.*, vol. 55, no. 1, pp. 132–139, Feb. 2013.

[22] D. Cavka, N. Mora, and F. Rachidi, "A comparison of frequency-dependent soil models: Application to the analysis of grounding systems," *IEEE Trans. Electromagn. Compat.*, vol. 56, no. 1, pp. 177–187, Feb. 2014.

[23] B. Gustavsen and A. Semlyen, "Rational approximation of frequency domain responses by vector fitting," *IEEE Trans. Power Del.*, vol. 14, no. 3, pp. 1052–1061, Jul. 1999.

[24] D. Deschrijver, M. Mrozowski, T. Dhaene, and D. De Zutter, "Macromodeling of multiport systems using a fast implementation of the vector fitting method," *IEEE Microw. Wireless Compon. Lett.*, vol. 18, no. 6, pp. 383–385, Jun. 2008.

[25] A. E. Ruehli, "Inductance calculations in a complex integrated-circuit environment," *IBM J. Res. Develop.*, vol. 16, no. 5, pp. 470–481, 1972.

[26] G. Antonini, S. Cristina, and A. Orlandi, "PEEC modeling of lightning protection systems and coupling to coaxial cables," *IEEE Trans. Electromagn. Compat.*, vol. 40, no. 4, pp. 481–491, Nov. 1998.

[27] D. Gope, A. Ruehli, and V. Jandhyala, "Solving low-frequency EM-CKT problems using the PEEC method," *IEEE Trans. Adv. Packag.*, vol. 30, no. 2, pp. 313–320, 2007.

[28] J. E. Garrett, *Advancements of the Partial Element Equivalent Circuit Formulation*. Lexington, KY, USA: Univ. Kentucky, 1997.

[29] S. A. Schelkunoff, "The electromagnetic theory of coaxial transmission lines and cylindrical shields," *Bell Syst. Tech. J.*, vol. 13, no. 4, pp. 532–579, 1934.

[30] A. E. Ruehli, G. Antonini, and L. J. Jiang, "Skin-effect loss models for time- and frequency-domain PEEC solver," *Proc. IEEE*, vol. 101, no. 2, pp. 451–472, Feb. 2013.

[31] H. Chen and Y. Du, "Model of ferromagnetic steels for lightning transient analysis," *IET Sci., Meas. Technol.*, pp. 8, 2017, doi: 10.1049/iet-smt.2017.0400.

[32] C. R. Paul, *Inductance: Loop and Partial*. Hoboken, NJ, USA: Wiley, 2011.
[33] A. M. Mousa, "The soil ionization gradient associated with discharge of high currents into concentrated electrodes," *IEEE Trans. Power Del.*, vol. 9, no. 3, pp. 1669–1677, Jul. 1994.
[34] K. Jonguk, K. Hyun-Tai, K. Kwi-Soo, L. Jong-Sik, and A. Dal, "An equivalent circuit model for multi-port networks," in *Proc. Eur. Microw. Conf.*, 2007, pp. 901–904.
[35] A. C. Lima, B. Gustavsen, and A. B. Fernandes, "Inaccuracies in network realization of rational models due to finite precision of RLC branches," in *Proc. Int. Conf. Power Syst. Transients*, 2007, pp. 4–7.
[36] G. Antonini, "SPICE equivalent circuits of frequency-domain responses," *IEEE Trans. Electromagn. Compat.*, vol. 45, no. 3, pp. 502–512, Aug. 2003.
[37] A. Geri, "Behaviour of grounding systems excited by high impulse currents: The model and its validation," *IEEE Trans. Power Del.*, vol. 14, no. 3, pp. 1008–1017, Jul. 1999.
[38] Z. Stojkovic, M. S. Savic, J. M. Nahman, D. Salamon, and B. Bukorovic, "Sensitivity analysis of experimentally determined grounding grid impulse characteristics," *IEEE Trans. Power Del.*, vol. 13, no. 4, pp. 1136–1142, Oct. 1998.
[39] Protection of Structures Against Lightning: Part I General *P*rinciples, IEC Standard 62305-1, 2010.
[40] F. Heidler, J. M. Cvetic, and B. V. Stanic, "Calculation of lightning current parameters," *IEEE Trans. Power Del.*, vol. 14, no. 2, pp. 399–404, Apr. 1999.

Hongcai Chen (S'17) received the B.S. degree in electronic science and technology from the Hefei University of Technology, Hefei, China, in 2012. He is currently working toward the Ph.D. degree in electrical engineering at the Hong Kong Polytechnic University, Hong Kong.

From February 2017 to August 2017, he was a Visiting Scholar at Duke University, Durham, NC, USA. He is currently developing an integrated software for analyzing transient current distribution in power systems. His current research interests include electromagnetic transient analysis, computational electromagnetics, and grounding system in complex media.

Yaping Du received the B.S. and M.S. degrees in electrical engineering from Shanghai Jiao Tong University, Shanghai, China, in 1984 and 1987, respectively, and the Ph.D. degree in electrical engineering from the University of Southern California, Los Angeles, CA, USA, in 1994.

He is currently a Professor with the Department of Building Services Engineering, the Hong Kong Polytechnic University, Hong Kong. His research interests include electromagnetic environments, lightning protection, and power quality in electric power systems, electrified railway systems, and buildings.

Dr. Du is a member of the Institution of Electrical Engineers, and a Chartered Engineer of the U.K.